Computational Chemistry

DOI: 10.1002/anie.201204116

Model and Mechanism: N-Hydroxylation of Primary Aromatic Amines by Cytochrome P450**

*Li Ji and Gerrit Schüürmann**

Primary aromatic amines (PAA) are used for the synthesis of various products including pesticides, pharmaceuticals, rubber, azo dyes, epoxy polymers, and aromatic polyurethane materials, and are thus of considerable industrial interest.[1] Their potential mutagenicity and carcinogenicity have been recognized to be initiated through N-hydroxylation by cytochrome P450 enzymes (P450).[2] The underlying reaction mechanism, however, is still a matter of debate. So far, four pathways involving the active-site ferryl oxo species $Fe^{IV}O$ called Compound I (Cpd I)[3] and one route catalyzed by the ferric peroxo dianion $Fe^{III}OO^{2-}$[4] have been discussed (Scheme 1 a–e): a) H-atom transfer (HAT), involving H-atom abstraction from the amine N by the FeO oxygen center and a subsequent radical rebound step to yield the aromatic hydroxylamine ArNHOH; b) oxygen addition rearrangement (OAR), wherein the FeO oxygen atom adds at the N lone pair with subsequent rearrangement to the hydroxylamine; c) single-electron transfer (SET) from the amine to FeO with subsequent proton transfer and a final rebound step between the intermediate aminyl radical and FeOH; d) two-electron transfer (TET), of which only the variant with the maximum number of elementary steps (SET + proton transfer + SET + rebound) is shown in the scheme; and e) proton transfer (PT) to $FeOO^{2-}$ to form the ferric hydroperoxide anion $FeOOH^-$ (Cpd 0) and $ArNH^-$, thus eventually leading to ArNHOH upon protonation.

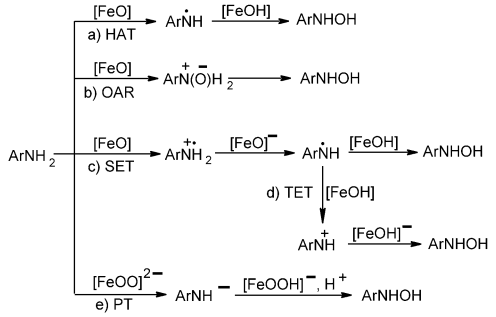

Scheme 1. Alternative mechanisms for the N-hydroxylation of primary aromatic amines by P450. HAT: H atom transfer; OAR: oxygen addition rearrangement; SET: single-electron transfer; TET: two-electron transfer; PT: proton transfer.

Computational analysis of enzyme catalysis such as P450 oxygenation has shed new light on the features of the electronic structure governing reactivity, and complements experimental information.[5] Earlier theoretical investigations of the P450 catalysis concerned the hydroxylation of C–H bonds,[6] the epoxidation of C=C bonds,[7] and the oxidation of heteroatoms.[8] Cpd I in the active site of P450 was shown to have two close-lying electronic states, a high-spin (HS) quartet state and a low-spin (LS) doublet state, which may contribute differently to various reactions.[5] So far, the mechanism underlying the PAA hydroxylation is unclear with regard to which of the above-outlined five pathways is energetically preferred, and whether one or more spin states contribute significantly to this toxicologically important metabolic conversion.

To clarify this issue, Gaussian 03[9] density functional theory (DFT) calculations have been undertaken without and with simulated solvation (PCM = polarized continuum-solvation model; see Methods Section) by employing the six-coordinated oxo-ferryl species $Fe^{4+}O^{2-}(Por)^-(SH)^-$ (with Por = porphyrin = $C_{20}N_4H_{12}$) as a model for Cpd I,[5,10] and $Fe^{3+}OO^{2-}(Por)^{2-}SH^-$ as a model for the active-site peroxo-dianion base as a precursor of Cpd 0 (ferric hydroperoxo complex) which in turn precedes Cpd I in the catalytic cycle.[5a] The COSMO[11] continuum-solvation model in the Gaussian CPCM implementation has also been tested, and provided nearly the same results as PCM. Besides aniline ($C_6H_5NH_2$), three *para*-substituted derivatives (*p*-CN, *p*-Cl, *p*-Me) were included to enable comparison with experimental data.[12]

For the SET and TET mechanisms involving Cpd I (Scheme 1 c and d), the activation barriers ($\Delta G^{\neq}$) have been calculated using the Marcus theory[13] (see the Supporting Information; a more elaborate approach would be constrained DFT simulations[14] combining electron-transfer kinetics and dynamics). In the HS and LS spin state, the SET $\Delta G^{\neq}$ [kcal mol^{-1}] values are 248.6/242.5 for aniline, 191.8/187.9 for *p*-Me aniline, 223.5/219.0 for *p*-Cl aniline, and 272.1/266.2 for *p*-CN aniline. The corresponding $\Delta G^{\neq}$ values calculated for the TET pathway are 248.6/242.5 (aniline), 191.8/187.9 (*p*-Me), 223.5/219.0 (*p*-Cl), and 272.1/266.2 (*p*-

[*] L. Ji, Prof. Dr. G. Schüürmann
UFZ Department of Ecological Chemistry
Helmholtz Centre for Environmental Research
Permoserstrasse 15, 04318 Leipzig (Germany)
and
Institute for Organic Chemistry
Technical University Bergakademie Freiberg
Leipziger Strasse 29, 09596 Freiberg (Germany)
E-mail: gerrit.schuurmann@ufz.de

[**] This work was supported by the China Scholarship Council (No. 2008619025) and the EU project OSIRIS (No. GOCE-CT-2007-037017). L.J. thanks D. Wondrousch and R. Stüwe for providing technical help.

Supporting information for this article is available on the WWW under http://dx.doi.org/10.1002/anie.201204116.

CN). These very large activation barriers suggest that an electron-transfer mechanism can be ruled out as relevant pathway for the P450-catalyzed N-hydroxylation of PAA.

Additional support for this conclusion is given by the experimental observation that the rates of NADPH consumption and hydroxylamine formation of these anilines did not show a significant dependence on the *para* Hammett constant,[12] thus indicating a lack of substantial charge build-up in the rate-determining step. Moreover, the experimental[15] ionization potentials (IP) of aniline and its *p*-Me, *p*-Cl, and *p*-CN derivatives are 7.73, 7.85, 7.80, and 8.64 eV respectively, thus contrasting with a much lower electron affinity (EA) of only 3.06 eV for Cpd I.[16] For the anilino radical and the *p*-substituted derivatives, our DFT calculations yield gas-phase vertical IP [eV] values of 8.05, 7.67 (*p*-Me), 7.97 (*p*-Cl), and 8.54 (*p*-CN), and a vertical EA of 2.58 eV for FeOH (Cpd I). These data provide further evidence that the SET and TET pathways are unlikely to provide a significant contribution.

Regarding the FeO-catalyzed HAT and OAR pathways (Scheme 1 a and b), the calculated LS and HS energy profiles for the reaction of aniline with Cpd I are shown in Scheme 2 together with geometric details of the relevant molecular species. The initially formed LS and HS reactant complexes (^{2,4}RC) with hydrogen bonding between one H on the nitrogen atom of aniline and the $Fe^{IV}O$ oxygen center of Cpd I are shown in the middle of the scheme. The HAT and OAR pathways proceed to the right and left, respectively, of ^{2,4}RC in the depiction. In the ^{2,4}RC species, the Cpd I moiety has a spin density of about two on the FeO unit, and one on the Por + SH fragment. This spin distribution is in accord with the triradicaloid Fe^{IV} HS and LS states of Cpd I as described by a CASPT2/MM approach.[17] On the HS surface of the HAT route, a small H-abstraction barrier (^4TS_H) of 3.2 kcal mol^{-1} in the PCM-simulated protein environment (3.8 kcal mol^{-1} in the gas phase) leads to an intermediate ($^4C_{IH}$) consisting of an iron-hydroxo group (PorFe^{IV}OH) with a closed-shell porphyrin (whose spin density is −0.12 as opposed to 0.44 in ^{4}RC, thus indicating a prevalence of Fe^{IV} over Fe^{III} in $^4C_{IH}$)[5a,18] and an anilino radical (PhNH•), followed by a considerable rebound barrier of 13.2 kcal mol^{-1} to cross the transition state ($^4TS_{reb}$) before reaching the product ($^4P_{OH}$) as the complex of the ferric iron porphyrin (Por-Fe^{III}) and the N-hydroxylamine (PhNHOH). The height of this HS barrier implies that ^{4}Cpd I will be a sluggish oxidant and unlikely to play a key role in the HAT.

The respective LS pathway yields a qualitatively different picture. Here, the product complex $^2P_{OH}$ is formed in a concerted manner from the reactant complex ^{2}RC through a tiny H-abstraction barrier (^2TS_H) of 3.7 kcal mol^{-1} (protein environment).

The fact that the HS rebound barrier ($^4TS_{reb}$) is higher than both the H-abstraction barriers for HS and LS (^4TS_H and ^2TS_H) contrasts with the energy profile found for the aliphatic C–H hydroxylation mechanism, where the energy of $^4TS_{reb}$ was always much lower than that of both ^4TS_H and ^2TS_H.[5a] To the best of our knowledge, the largest C–H hydroxylation rebound barrier calculated so far was obtained for the HS surface of the α-CH hydroxylation of *N*-nitrosodimethylamine (11.2 kcal mol^{-1}),[18] which was, however, still much lower than the respective initial spin-averaged H-abstraction barrier (16.6 kcal mol^{-1}).

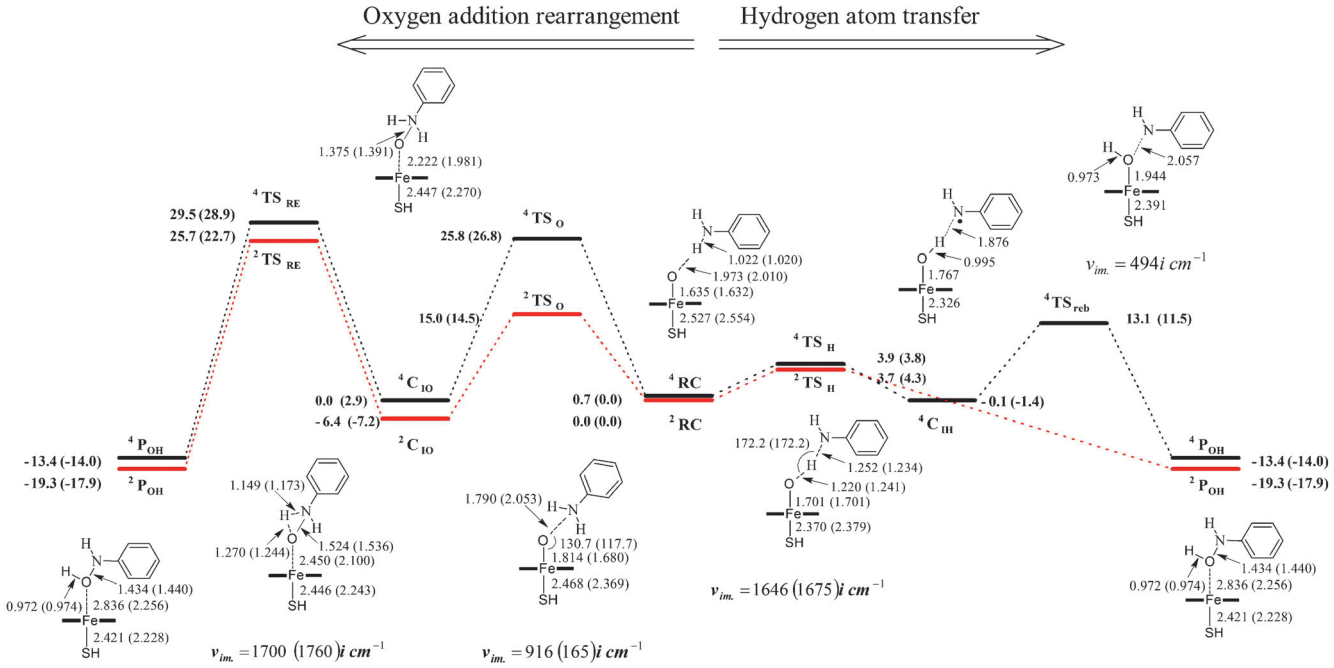

Scheme 2. Energy profiles (UB3LYP/BSII//BSI) and geometric details [distances in Å, angles in degrees, given in order HS (LS)] for the HAT and OAR N-hydroxylation of aniline by Cpd I in HS and LS states. Energies (in kcal mol^{-1}) are given relative to ^{2}RC with PCM ($\varepsilon = 5.6$) + ZPE, with gas-phase values in parentheses. ^{4,2}RC = quartet and doublet reactant complex, TS_H = transition state of H-abstraction, C_{IH} = intermediate complex with H abstracted by Cpd I, TS_{reb} = rebound transition state, TS_O = transition state of O addition, C_{IO} = N-oxide intermediate complex, TS_{RE} = transition state of H rearrangement, P_{OH} = N-hydroxylamine product complex. For transition states, the imaginary frequencies are shown.

For the *p*-substituted anilines, the relevant reaction barriers of the N–H abstraction (^4TS_H, ^2TS_H) and rebound step ($^4TS_{reb}$) are listed in Table 1 (together with the corresponding values for aniline). As with aniline, the HS rebound barrier is much larger than the LS H-abstraction barrier which is in turn slightly above its HS counterpart, thus implying that only the LS channel will contribute significantly to the HAT pathway of the primary amine N-hydroxylation. Moreover, increasing the electron-attraction power of the aniline substituent as quantified through the Hammett constants (from $\sigma_{para} = -0.17$ for Me to $\sigma_{para} = 0.66$ for CN) increases the H-abstraction barrier for both the LS and HS state, thus yielding a good correlation with an r^2 value of 0.987 ($\Delta E^{\neq}$ (spin-averaged, PCM) $= 8.736\,\sigma_{para} + 2.934$).

Table 1: Activation energies (in kcal mol^{-1}) for the HAT and OAR reactions of aniline and *p*-substituted anilines with Cpd I of P450.[a]

	Aniline	*p*-Me	*p*-Cl	*p*-CN
UB3LYP/BSII//BSI + ZPE				
$^4TS_H/^2TS_H$	3.8/4.3	2.1/2.5	4.3/4.8	7.3/8.1
$^4TS_{reb}$	12.9	10.0	11.8	15.3
$^4TS_O/^2TS_O$	26.8/14.5	25.8/13.6	27.9/15.9	31.1/19.4
$^4TS_{RE}/^2TS_{RE}$	26.0/29.9	26.3/30.1	25.8/29.5	24.8/28.5
UB3LYP/BSII//BSI + PCM solvation + ZPE				
$^4TS_H/^2TS_H$	3.2/3.7	0.8/1.4	4.7/4.9	8.5/8.8
$^4TS_{reb}$	13.2	10.5	13.3	17.4
$^4TS_O/^2TS_O$	25.1/15.0	23.9/14.0	26.5/16.9	30.3/20.6
$^4TS_{RE}/^2TS_{RE}$	29.5/32.1	29.6/31.9	29.6/31.0	28.7/30.1

[a] BSI = basis set I: LACVP (Fe), 6-31G* (O attached to Fe, four pyrrole N, amino N, thiol S), 6-31G (all other atoms); BSII = basis set II: LACVP (Fe), 6-31 + G** (all other atoms); PCM solvation with $\varepsilon = 5.62$ simulating the bulk protein environment.

The kinetic isotope effect (KIE) as a potential experimental HAT probe was calculated using the semi-classical Eyring model and its Wigner-corrected variant,[6b] thus yielding KIE values of 5.8 and 8.0 (^2TS_H) and of 5.7 and 7.8 (^4TS_H) with these two models, respectively (see the Supporting Information). Note also that the HAT can be understood as a particularly simple case of the PCET (proton-coupled electron transfer) class of reactions.[19] The consecutive PT/ET pathway would be highly endothermic concerning the initial PT by about 55 kcal mol^{-1} (PCM, $\varepsilon = 5.62$), and the ET/PT sequence can be ruled out because of the very large ET barrier as discussed above.

The energy profile of the alternative OAR pathway of the N-hydroxylation is shown in Scheme 2 (left-hand side). Here, the initial O addition to the N lone pair is more favorable by 10.1 kcal mol^{-1} (PCM protein environment) in the LS state (^2TS_O) than it is in the HS state (^4TS_O). Accordingly, the N-oxide as an intermediate complex will be formed mainly in the LS state ($^2C_{IO}$), and is in line with other heteroatom oxidation reactions.[8] The latter holds also for the transition-state geometries, where the Fe-O-$N_{aniline}$ angle is clearly larger for ^4TS_O (130.7°) than for ^2TS_O (117.7°).

Subsequently, H rearrangement converts the N-oxide ($^{4(2)}C_{IO}$) into the hydroxylamine product ($^{4(2)}P_{OH}$). The associated activation barrier is still larger than that for the preceding O addition, with PCM values of 32.1 and 29.5 kcal for the LS ($^2TS_{RE}$) and HS ($^4TS_{RE}$) state, respectively. It follows that this H rearrangement would represent the overall rate-determining step of the OAR pathway, with a reaction barrier higher by more than 25 kcal mol^{-1} relative to the one for the H abstraction as the rate-determining step of the LS state, HAT pathway. For the *p*-Me, *p*-Cl, and *p*-CN derivatives, the respective results are summarized in Table 1.

Overall, the results demonstrate that for the N-hydroxylation of primary aromatic amines, the OAR pathway cannot compete with the HAT pathway because the energy demand of its rate-determining step is larger by more than 20 kcal mol^{-1}. Moreover, the HAT pathway clearly prefers the LS route because of its lack of a rebound barrier, and in this respect resembles the C–H hydroxylation of alkanes[5a] as well as of *N*,*N*-dialkyl nitrosamines.[18]

To check whether the present results depend on the choice of B3LYP, the corresponding calculations for the N-hydroxylation of aniline were run with B3PW91, BLYP, BP86, PBE, TPSS, and B97D which includes a dispersion correction.[20] With all of these DFT functionals, the same qualitative picture, including a clear energetic preference for the HAT mechanism in the LS route, was obtained (see the Supporting Information), thus supporting the presently derived conclusions.

Recently, the involvement of Cpd I in the N-hydroxylation of aromatic amines has been questioned.[4] Because of geometric constraints imposed by hydrogen bonding between the active-site Thr124 (threonine) and the substrate amino N, it was concluded that only for $FeOO^{2-}$ could a distance close enough to the substrate for reaction be reached. Accordingly, a proton transfer from $ArNH_2$ to $FeOO^{2-}$ was proposed as the initial step of this alternative N-hydroxylation pathway (Scheme 1e), and supported thermodynamically by suitable proton affinities ($FeOO^{2-}$: 422 kcal mol^{-1}, $ArNH_2$: 350–390 kcal mol^{-1}).

However, our attempts to locate a respective PT transition state without and with a two-water bridge through reaction-path calculations failed. Instead, geometry optimization of Cpd I with aniline in the P450 1A2 protein environment represented by most of its first-shell amino acid residues yielded the complex shown in Scheme 3. The latter reveals an hydrogen bond between Thr124 and the aniline ring, thus

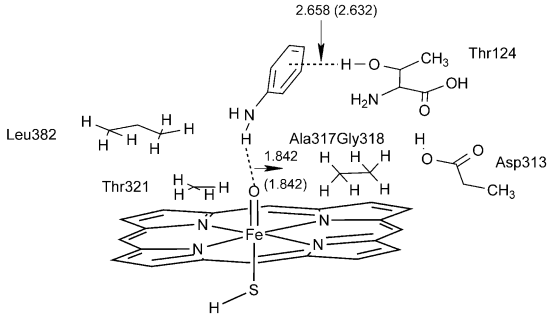

Scheme 3. Geometry-optimized complex between Cpd I and aniline in the P450 1A2 active site. Geometric parameters (lengths are in Å) are given in the order: HS (LS).

allowing the aniline N to come sufficiently close to Cpd I ($FeO\cdots H_2NAr$ distance = 1.84 Å) for initiating an H abstraction as the first step of the HAT mechanism [Scheme 1a, and Scheme 2 (right-hand side)]. Calculation of the HAT barrier in this protein environment yielded 3.4 kcal mol^{-1} for both HS and LS (PCM + ZPE), and is similar to the results without first-shell amino acids. It follows that Cpd I is geometrically available for catalyzing the N-hydroxylation of PAA, and that the above-discussed HAT mechanism is kinetically preferred over all alternative pathways discussed so far.

A further implication of the present analysis concerns the possible formation of N-oxides during the P450-catalyzed biotransformation of primary aromatic amines. While N-oxide metabolites had been found in liver microsomes after exposure to tertiary amines,[21] we are not aware of respective reports for primary amines. Indeed, the relatively low difference in activation energies as calculated for the N-oxide formation and α-CH hydroxylation of *N*,*N*-dimethyl aniline (6.09 kcal mol^{-1})[8c] and trimethylamine (2.90 and 4.45 kcal mol^{-1})[8b,c] make a competition between both pathways for tertiary aliphatic and aromatic amines reasonable. In contrast, our present results show that in the case of primary aromatic amines, the reaction barrier for the O addition (as first step of the OAR N-hydroxylation pathway) is approximately 12.5 kcal mol^{-1} higher than for the H abstraction (as first HAT step). Accordingly, the probability of N-oxide formation appears to be too low because of its too large energy demand as compared to the alternative H abstraction, thus explaining the lack of respective experimental findings.

For both the H abstraction of alkanes and at the α-C of *N*,*N*-dialkyl nitrosamines as a first step of the P450-catalyzed C–H hydroxylation, the calculated (spin-averaged) reaction barriers were shown to correlate with the C–H bond dissociation energies (BDE) of the isolated substrates.[18,22] A similar situation holds for primary aromatic amines, thus yielding a good correlation between their (spin-averaged) H-abstraction barriers and experimental N–H BDE values determined electrochemically[23] ($r^2 = 0.9$). It follows that also for these compounds, BDEs offer a short-cut approach for a screening-level estimation of their barriers of P450-catalyzed H abstraction from N.

As compared to alkane, benzylic and allylic C–H with calculated H-abstraction barriers of 14–23, 13 (toluene), and just below 11 kcal mol^{-1} (propene),[22] the energy demand for the H abstraction from the aniline N–H is much lower with a spin-averaged barrier of only 3.5 kcal mol^{-1} (Scheme 2 and Table 1). The latter is in accord with the experimental finding that the metabolic conversion of anilines belongs to the fastest P450-catalyzed reactions.[24] Interestingly, however, the H-abstraction barrier of toluene is much larger than the one of aniline, although the N–H BDE of aniline (89.1–92.3 kcal mol^{-1})[25] and the C–H BDE of toluene (87.9–90.4 kcal mol^{-1})[26] are quite similar. Recalculation of the toluene HAT barrier with our computational setting yields HS values with and without PCM ($\varepsilon = 5.62$) of 13.7 and 12.7 kcal mol^{-1} (the corresponding LS values are 11.8 and 12.0 kcal mol^{-1}), and thus a spin-averaged increase of 9.3 (PCM) kcal mol^{-1} over the aniline HAT barrier.

Why is aniline much more reactive under P450 catalysis than toluene toward H abstraction despite similar bond strengths of the H atom as quantified through the respective BDE values? Inspection of the electronic structure of the corresponding HS transition states offers the following explanations (keeping in mind that DFT-based electronic structure details of the LS state appear to be generally less reliable[7a]): First, with aniline as a P450 substrate, the Mulliken spin density of the developing anilino radical (PhNH$^{\bullet}$) is 0.78 in the ^4TS_H, but only 0.54 in the benzyl radical ($PhCH_2^{\bullet}$), and the respective values for anilino N and benzylic C are 0.46 and 0.43, respectively. Thus, the phenyl ring of aniline participates much more strongly in the reorganization of the electronic structure, thereby facilitating the homolytic H abstraction through stabilization of the developing radical.

Second, at the TS the temporary electron transfer to Cpd I from aniline amounts to 0.50 (NBO charge) as opposed to 0.29 from toluene, and reduces to 0.05 (anilino radical) and 0.01 (benzyl radical) in the subsequent intermediate complex ($^4C_{IH}$). The lower ionization potential of aniline as compared to toluene (vertical: 7.83 vs. 8.80 eV) makes the aromatic amine more susceptible for this HAT assistance. Note that while the SET and TET pathways of the PAA N-hydroxylation are energetically not feasible, the HAT pathway appears to involve temporary partial charge-transfer assistance, thus enriching the otherwise homolytic H-abstraction mechanism.

As compared to PAA, primary aliphatic amines have higher HAT barriers and lower OAR barriers.[27] The latter can be explained by the larger nucleophilicity of aliphatic N (e.g. NBO charge propan-2-amine versus aniline: −0.853 versus −0.792). Regarding the former, calculation of the HAT barrier for propane-2-amine with our present approach yields HS results with and without PCM of 11.1 and 9.5 kcal mol^{-1} (thus clearly exceeding the corresponding aniline values listed in Table 1; the corresponding LS values are 11.3 and 10.0 kcal mol^{-1}). The developing spin in the aliphatic radical RNH$^{\bullet}$ is mainly localized at N (0.73) as opposed to a pronounced spin delocalization in the anilino radical. Accordingly, aromatic delocalization can explain the strong preference of PAA for HAT as opposed to primary aliphatic amines which are similarly susceptible to OAR and HAT.

In conclusion, our computational analysis of the N-hydroxylation of primary aromatic amines reveals that among the five mechanistic options discussed so far,[3,4] the SET and TET pathways appear to be impossible because of extremely high reaction barriers of greater than 180 kcal mol^{-1}, and that the OAR pathway can also be ruled out because of a rate-determining barrier of approximately 30 kcal mol^{-1} as compared to less than 9 kcal mol^{-1} for the HAT pathway. Moreover, the recently proposed PT pathway involving $FeOO^{2-}$ appears to be less likely, both because of an apparently strong kinetic resistance of $ArNH_2$ to donate a proton, and because Cpd I is in fact geometrically available for reacting with PAA as opposed to previous conclusions.[4] Thus, the HAT pathway is kinetically preferred over all alternative mechanisms discussed so far, thus offering a concerted LS N-hydroxylation with a barrier-free oxygen rebound step.

Computational Methods

The DFT calculations were performed with Gaussian 03[9] except for the B97D functional for which Gaussian 09[28] was used. Cpd I of the P450 active site was modeled as six-coordinated triradicaloid oxoferryl complex $Fe^{4+}O^{2-}(C_{20}N_4H_{12})^{-}(SH)^{-} \equiv FeO$, with $C_{20}N_4H_{12}$ = porphyrin = Por. Geometry optimization was carried out using the unrestricted B3LYP functional with the following basis set denoted BSI: effective core potential plus LACVP (LANL2DZ) on Fe, 6-31G* on seven further heteroatoms (O atom attached to Fe, four pyrrole N atoms, amino N, thiol S), and 6-31G for all remaining atoms. More accurate energies were determined by single-point calculations with LACVP (Fe) and 6-31 + G** (all other atoms), which is denoted BSII. Bulk protein environment was simulated with the PCM continuum-solvation model ($\varepsilon = 5.62$, chlorobenzene) at the UB3LYP/BSI level. ZPE (zero-point energy) corrections are based on UB3LYP/BSI frequency calculations. IP was calculated using B3LYP/aug-cc-pVTZ//6-311 + + G**, and for EA of FeOH(PorSH) B3LYP/LACVP-6-31 + G**//LACVP-6-31G was employed. For additional UB3LYP/LACVP-6-31G calculations with Cpd I in the relevant protein environment of P450 1A2 covering most first-shell amino acid residues Thr-124, Asp-313, Ala-317, Gly-318, Thr-321, and Leu-382 taken from crystal structure 2HI4 (PDB code), the structural composition of all residues except Thr-124 was simplified as described in the Supporting Information.

Received: May 27, 2012
Revised: August 4, 2012
Published online: November 21, 2012

Keywords: computational chemistry · cytochrome P450 · enzyme catalysis · hydrogen transfer · reaction mechanisms

[1] a) J. L. Radomski, *Annu. Rev. Pharmacol. Toxicol.* **1979**, *19*, 129 – 157; b) S. K. Mortensen, X. T. Trier, A. Foverskov, J. H. Petersen, *J. Chromatogr. A* **2005**, *1091*, 40 – 50.

[2] D. Kim, F. P. Guengerich, *Annu. Rev. Pharmacol. Toxicol.* **2005**, *45*, 27 – 49.

[3] a) G. J. Hammons, F. P. Guengerich, C. C. Weis, F. A. Beland, F. F. Kadlubar, *Cancer Res.* **1985**, *45*, 3578 – 3585; b) J. C. Sasaki, R. S. Fellers, M. E. Colvin, *Mutat. Res.* **2002**, *506 – 507*, 79 – 89.

[4] I. Shamovsky, L. Ripa, L. Borjesson, C. Mee, B. Norden, P. Hansen, C. Hasselgren, M. O'Donovan, P. Sjo, *J. Am. Chem. Soc.* **2011**, *133*, 16168 – 16185.

[5] a) S. Shaik, D. Kumar, S. P. de Visser, A. Altun, W. Thiel, *Chem. Rev.* **2005**, *105*, 2279 – 2328; b) S. Shaik, S. Cohen, Y. Wang, H. Chen, D. Kumar, W. Thiel, *Chem. Rev.* **2010**, *110*, 949 – 1017.

[6] a) F. Ogliaro, N. Harris, S. Cohen, M. Filatov, S. P. de Visser, S. Shaik, *J. Am. Chem. Soc.* **2000**, *122*, 8977 – 8989; b) S. P. de Visser, F. Ogliaro, P. K. Sharma, S. Shaik, *J. Am. Chem. Soc.* **2002**, *124*, 11809 – 11826; c) C. Li, W. Wu, D. Kumar, S. Shaik, *J. Am. Chem. Soc.* **2006**, *128*, 394 – 395; d) S. Shaik, D. Kumar, S. P. de Visser, *J. Am. Chem. Soc.* **2008**, *130*, 14016 – 14016.

[7] a) S. P. de Visser, F. Ogliaro, N. Harris, S. Shaik, *J. Am. Chem. Soc.* **2001**, *123*, 3037 – 3047; b) S. P. de Visser, F. Ogliaro, S. Shaik, *Angew. Chem.* **2001**, *113*, 2955 – 2958; *Angew. Chem. Int. Ed.* **2001**, *40*, 2871 – 2874; c) D. Kumar, B. Karamzadeh, G. N. Sastry, S. P. de Visser, *J. Am. Chem. Soc.* **2010**, *132*, 7656 – 7667.

[8] a) C. Li, L. Zhang, C. Zhang, H. Hirao, W. Wu, S. Shaik, *Angew. Chem.* **2007**, *119*, 8316 – 8318; *Angew. Chem. Int. Ed.* **2007**, *46*, 8168 – 8170; b) P. Rydberg, U. Ryde, L. Olsen, *J. Chem. Theory Comput.* **2008**, *4*, 1369 – 1377; c) C. Li, W. Wu, K. B. Cho, S. Shaik, *Chem. Eur. J.* **2009**, *15*, 8492 – 8503; d) S. Shaik, Y. Wang, H. Chen, J. S. A. Song, R. Meir, *Faraday Discuss.* **2010**, *145*, 49 – 70.

[9] M. J. Frisch et al., Gaussian 03, revision C.02; Gaussian, Inc.: Wallingford, CT, **2004**. See the Supporting Information.

[10] a) H. M. Senn, W. Thiel, *Angew. Chem.* **2009**, *121*, 1220 – 1254; *Angew. Chem. Int. Ed.* **2009**, *48*, 1198 – 1229; b) A. Franke, C. Fertinger, R. van Eldik, *Angew. Chem.* **2008**, *120*, 5316 – 5320; *Angew. Chem. Int. Ed.* **2008**, *47*, 5238 – 5242.

[11] A. Klamt, G. Schüürmann, *J. Chem. Soc. Perkin Trans. 2* **1993**, 799 – 805.

[12] J. N. Burstyn, M. Iskandar, J. F. Brady, J. M. Fukuto, A. K. Cho, *Chem. Res. Toxicol.* **1991**, *4*, 70 – 76.

[13] R. A. Marcus, *Angew. Chem.* **1993**, *105*, 1161 – 1172; *Angew. Chem. Int. Ed. Engl.* **1993**, *32*, 1111 – 1121.

[14] B. Kaduk, T. Kowalczyk, T. Van Voorhis, *Chem. Rev.* **2012**, *112*, 321 – 370.

[15] E. Klein, V. Lukes, Z. Cibulkova, J. Polovkova, *J. Mol. Struct. Theochem* **2006**, *758*, 149 – 159.

[16] F. Ogliaro, S. P. de Visser, S. Shaik, *J. Inorg. Biochem.* **2002**, *91*, 554 – 567.

[17] H. Chen, J. S. Song, W. Z. Lai, W. Wu, S. Shaik, *J. Chem. Theory Comput.* **2010**, *6*, 940 – 953.

[18] L. Ji, G. Schüürmann, *J. Phys. Chem. B* **2012**, *116*, 903 – 912.

[19] M. H. V. Huynh, T. J. Meyer, *Chem. Rev.* **2007**, *107*, 5004 – 5064.

[20] S. Grimme, *J. Comput. Chem.* **2006**, *27*, 1787 – 1799.

[21] P. Hlavica, *Drug Metab. Rev.* **2002**, *34*, 451 – 477.

[22] S. P. de Visser, D. Kumar, S. Cohen, R. Shacham, S. Shaik, *J. Am. Chem. Soc.* **2004**, *126*, 8362 – 8363.

[23] F. G. Bordwell, X. M. Zhang, J. P. Cheng, *J. Org. Chem.* **1993**, *58*, 6410 – 6416.

[24] a) J. M. Dady, S. P. Bradbury, A. D. Hoffman, M. M. Voit, D. L. Olson, *Xenobiotica* **1991**, *21*, 1605 – 1620; b) D. J. Mccarthy, W. R. Waud, R. F. Struck, D. L. Hill, *Cancer Res.* **1985**, *45*, 174 – 180; c) I. Golly, P. Hlavica, *Biochim. Biophys. Acta Protein Struct. Mol. Enzymol.* **1987**, *913*, 219 – 227.

[25] D. A. Pratt, G. A. DiLabio, L. Valgimigli, G. F. Pedulli, K. U. Ingold, *J. Am. Chem. Soc.* **2002**, *124*, 11085 – 11092.

[26] D. A. Pratt, J. S. Wright, K. U. Ingold, *J. Am. Chem. Soc.* **1999**, *121*, 4877 – 4882.

[27] P. Rydberg, L. Olsen, *J. Chem. Theory Comput.* **2011**, *7*, 3399 – 3404.

[28] M. J. Frisch et al., Gaussian 09, revision B.01; Gaussian, Inc.: Wallingford, CT, **2010**. See the Supporting Information.

